Probabilistic Contact Estimation and Impact Detection for State Estimation of Quadruped Robots

Marco Camurri, *Student Member, IEEE*, Maurice Fallon, *Member, IEEE*, Stéphane Bazeille, *Member, IEEE*, Andreea Radulescu, *Member, IEEE*, Victor Barasuol, Darwin G. Caldwell, *Member, IEEE*, and Claudio Semini, *Member, IEEE*

***Abstract*—Reliable state estimation is crucial for stable planning and control of legged locomotion. A fundamental component of a state estimator in legged platforms is Leg Odometry, which only requires information about kinematics and contacts. Many legged robots use dedicated sensors on each foot to detect ground contacts. However, this choice is impractical for many agile legged robots in field operations, as these sensors often degrade and break. Instead, this paper focuses on the development of a robust Leg Odometry module, which does not require contact sensors. The module estimates the probability of reliable contact and detects foot impacts using internal force sensing. This knowledge is then used to improve the kinematics-inertial state estimate of the robot's base. We show how our approach can reach comparable performance to systems with foot sensors. Extensive experimental results lasting over 1 h are presented on our 85 kg quadrupedal robot HyQ carrying out a variety of gaits.**

***Index Terms*—Localization, multilegged robots, sensor fusion.**

I. Introduction

LEGGED robots present unique capabilities for traversing a multitude of rough terrains, where they can potentially outperform wheeled or tracked systems. The successful implementation of these capabilities depends on the robot's ability to generate viable body trajectories, using a self-estimated base state vector, computed on board and in real-time. A base state vector typically includes position, orientation, linear and angular velocities, and acceleration of the robot's base.

The essential sensor inputs for self-reliant base state estimation in legged robots typically include an Inertial Measurement Unit (IMU) — measuring accelerations and angular velocity — and joint encoders, which are used to compute position and velocity of the end effectors (*i.e.,* the robot's feet) through forward kinematics.

Manuscript received September 10, 2016; accepted December 27, 2016. Date of publication January 16, 2017; date of current version February 16, 2017. This paper was recommended for publication by Associate Editor R. Ozawa and Editor P. Rocco upon evaluation of the reviewers' comments. This work was supported by the Istituto Italiano di Tecnologia.

M. Camurri, A. Radulescu, V. Barasuol, D. G. Caldwell, and C. Semini are with the Department of Advanced Robotics, Istituto Italiano di Tecnologia, Genoa 16163, Italy (e-mail: marco.camurri@iit.it; andreea.radulescu@iit.it; victor.barasuol@iit.it; darwin.caldwell@iit.it; claudio.semini@iit.it).

M. Fallon is with the School of Informatics, University of Edinburgh, Edinburgh EH8 9YL, U.K. (e-mail: maurice.fallon@ed.ac.uk).

S. Bazeille is with the IRCCyN, Ecole des Mines de Nantes, Nantes 44300, France (e-mail: stephane.bazeille@mines-nantes.fr).

Color versions of one or more of the figures in this paper are available online at http://ieeexplore.ieee.org.

Digital Object Identifier 10.1109/LRA.2017.2652491

Reliable velocity estimates for the base can be extracted from the feet velocities expressed in the base frame, a technique known as Leg Odometry (LO) [1]. Typical approaches use constraints based on the knowledge of at least one secure (*i.e.,* non-slipping) contact between the feet and the ground. Detecting such a contact event is not trivial, as it depends on the amount of frictional force the foot exerts on the terrain [2]. According to the Coulomb model of dry friction, this is directly proportional to the normal component of the Ground Reaction Force (GRF) and the foot-terrain static friction coefficient, which is generally unknown. Additionally, impact forces play a critical role, as they can cause slippage [3] and exacerbate undesired compliances in the leg structure. Furthermore, when contact sensors at the feet are unavailable, the difficulty of the task increases, as an indirect estimate of the GRF is required.

This paper addresses these issues by providing a novel probabilistic method for the estimation of reliable contacts between the feet and the ground. In contrast to conventional contact estimation methods, which aim to detect the earliest moments of robot-environment interactions, we are interested in estimating the probability of contacts which can be used to minimize the base velocity error. Our method is based on the estimation of the GRF at foot level, which provides a measure of confidence that a foot is firmly in contact with the ground. With this information, the individual velocity contributions from the stance legs are fused into one base velocity estimate. To further improve the filter's performance, we also incorporate the effect of impacts in the computation of the uncertainty associated to the velocity estimate. Despite the absence of contact sensors, our method results in state-of-the-art performance on a dynamic quadruped robot, executing quasi-static and dynamic locomotion gaits.

We validate the performance of the method on the Hydraulic Quadruped (HyQ) [4], a dynamic platform capable of a variety of locomotion gaits, including trotting up to 2 ms^{-1} and multi-directional crawling. Fig. 1 depicts the HyQ platform and a schematic showing the coordinate frames used in this paper and feet naming conventions. We present results for the proposed estimator in a variety of dynamic and quasi-static locomotion experiments with a total duration of 62 min. To the best of our knowledge, this constitutes the most extensive, scientifically verified study of kinematics-inertial state estimation on heavy and dynamic legged systems.

The remainder of this paper is structured as follows: Section II overviews the relevant literature on the topic; Section III

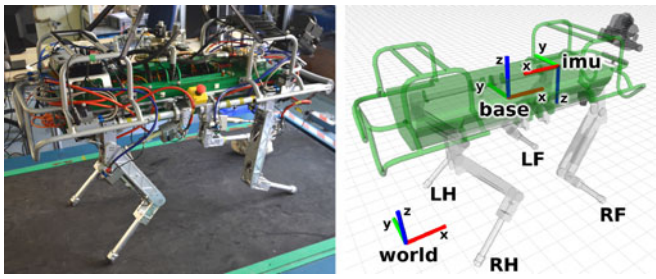

Fig. 1. *Left:* IIT's Hydraulic Quadruped robot (HyQ). *Right:* Summary of the coordinate frames and notations used in this paper: the Base frame is attached to the geometric center of the robot's torso and has the x-axis (red) pointing forward, the y-axis (green) pointing to the left, and the z-axis (blue) pointing upward; the IMU frame is also attached to the base link, with a different orientation; the World frame is a fixed reference frame. The legs are referred by the following abbreviations: LF (Left Front), RF (Right Front), LH (Left Hind), RH (Right Hind).

provides a formal definition of the proposed state estimation problem which does not require contact sensing; Section IV presents our approach to contact estimation; Section V describes how linear velocity measurement updates are created using this contact information; Section VI describes our experimental setup as well as extensive test results; in Section VII we discuss the effect of leg compliance on the experimental results and the algorithmic limitations of our approach; in Section VIII we conclude with a summary and some suggestions for future work.

II. Related Work

State estimation for legged robots is a widely studied problem. A variety of solutions have been proposed with different sensor combinations including [5]–[7]. We are however most interested in larger scale platforms, that can perform dynamic gaits, such as trotting or running, without contact sensors, and can carry a substantial payload. In this context, to the best of our knowledge, the available literature addresses either legged state estimation with contact sensors or contact/collision estimation without contact sensors.

A. Legged State Estimation With Contact Sensors

Recently, Blösch *et al.* [8] developed a state estimator that fuses leg kinematics and inertial information using an Extended Kalman Filter (EKF). The state vector includes the feet positions, whose uncertainty is used to account for moderate slippage and absence of ground contacts, which are detected with dedicated sensors. The validity of this approach was demonstrated on the medium-sized quadruped robot StarlETH [9] for a 1min straight crawl. Later [10], the same group extended their work by replacing the EKF with an Unscented Kalman Filter (UKF) and redefining the formulation of the state vector to be robot-centric (*i.e.,* expressed in the base frame). The velocity contributions of each leg readings are discarded if the filter innovation, expressed in Mahalanobis distance, exceeds a fixed threshold, found empirically. This procedure eliminates the effect of spurious filter updates originating from the legs whose contact state estimates are unreliable. As in [8], the performance of the approach was demonstrated on the StarlETH platform, for a $23\ \text{s}$ trot on a flat terrain made unstable and slippery by placing wooden debris along the way.

In [11], Fallon *et al.* presented Pronto: an efficient, modular and open-source EKF-based state estimator. The algorithm uses an IMU-based process model and combines this with measurement corrections from different sensor modalities (LO, LiDAR and vision) to produce a position estimate for the humanoid robot Atlas, developed by Boston Dynamics. In particular, the LO module handles contacts using a Schmitt trigger (a two threshold comparator with hysteresis, see [12]) on the contact sensor signals: the contact is detected when the low threshold is crossed and it is released when an arbitrary time has passed and the high threshold is crossed. When the robot is in double support, only one leg is used, for simplicity. The filter is able to handle out-of-order and asynchronous inputs from different sensors. Originally developed for the DARPA Robotics Challenge, its implementation has been recently released publicly.[1] We use this filtering framework as a basis of the sensor fusion presented herein. We have replaced the humanoid specific LO module with a quadrupedal specific approach, which uses the generated kinematics library of [13] and merges multiple leg contributions to create raw base velocity estimates.

Ma *et al.* [14] fuse (using an EKF) the information from a stereo camera, coupled to the leg kinematics and a tactical grade IMU. The state vector is defined as an error matrix (values propagated from the IMU against measurement updates). The approach is focused on visual inertial fusion with LO measurements expressed as delta positions between two key frames, used only in case of failure of the Visual Odometry (VO). The approach produced a robust performance with an error below 1% of the distance traveled when fused with GPS.

B. Contact/Collision Estimation Without Contact Sensors

Most research in the area of contact estimation is focused on collision avoidance for safe Human Robot Interaction (HRI) with manipulators. De Luca *et al.* [15] proposed a collision detection and reaction method which identifies external forces acting on a link as first order filtered external torques acting on the manipulator's joints. The reaction strategy typically involves stopping or moving the link away and along the direction of the identified contact. Haddadin *et al.* [16] extended this work by introducing a modified version of the contact detection, more recovery strategies, and by extensively experimenting with a human subject.

More recently, Hwangbo *et al.* [17] developed a probabilistic contact estimator to control the quadruped electric robot ANYmal without foot sensors. The method fuses information about dynamics, differential kinematics and kinematics using a method similar to a Hidden Markov Model (HMM) to reconstruct the contact status. The validity of this approach was demonstrated by comparing their method with Generalized Momentum (GM) approaches, using the delay detected by OptoForce sensors as a metric.

[1] https://github.com/ipab-slmc/pronto-distro

It has to be noted that the contact detection methods presented above aim to detect the contact as early as possible, in order to promptly take counter measures against unwanted collisions [15], [16] or to control the robot [17]. In contrast, we are interested in detecting the first instant of a leg's contact phase from which a reliable and trustworthy velocity measure can be produced, which is a substantially different goal. This is achieved by: 1) learning the threshold of the normal component of the GRF that minimizes the velocity error; 2) incorporating impact information and consistency between feet velocity estimates in the covariance associated to the measurement update of the filter.

III. Problem Definition

The robot base state vector is defined by:

$$\mathcal{X} = \begin{bmatrix} {}_w\mathbf{x}_b & {}_b\dot{\mathbf{x}}_b & {}_b\ddot{\mathbf{x}}_b & {}_w\boldsymbol{\theta}_b & {}_b\boldsymbol{\omega}_b & \mathbf{b}_a & \mathbf{b}_\omega \end{bmatrix} \quad (1)$$

where the base velocity ${}_b\dot{\mathbf{x}}_b$, acceleration ${}_b\ddot{\mathbf{x}}_b$ and rotational rate ${}_b\boldsymbol{\omega}_b$ are expressed in the base frame b, while the position ${}_w\mathbf{x}_b$ and orientation ${}_w\boldsymbol{\theta}_b$ are expressed in the fixed world frame w. The state vector is completed by IMU acceleration/angular velocity biases $\mathbf{b}_a$, $\mathbf{b}_\omega$, and is updated by an EKF, from [11].

Measurements of acceleration and angular velocity are taken from the IMU at 500 Hz. These are transformed into the base frame to produce direct measurements of the base acceleration ${}_b\ddot{\mathbf{x}}_b$ and angular velocity ${}_b\boldsymbol{\omega}_b$ as follows:

$${}_b\boldsymbol{\omega}_b = R^b_i\, {}_i\boldsymbol{\omega}_b = R^b_i\, {}_i\boldsymbol{\omega}_i \quad (2)$$

$${}_b\ddot{\mathbf{x}}_b = R^b_i\, {}_i\ddot{\mathbf{x}}_i - {}_b\mathbf{g} \quad (3)$$

where R^i_b is the rotation matrix from IMU frame i to the base frame b. In (3), we assume the effects of angular acceleration and centripetal force (see [18]) to be negligible. The EKF is then propagated using a direct inertial process model.

During the filter update step, a measure for the base velocity ${}_b\dot{\mathbf{x}}_b$ is computed by fusing a kinematic contribution ${}_b\dot{\mathbf{x}}_{b_l}$ from each foot f_l, as follows:

$${}_b\dot{\mathbf{x}}_{b_l} = -{}_b\dot{\mathbf{x}}_{f_l} - {}_b\boldsymbol{\omega}_b \times {}_b\mathbf{x}_{f_l} \quad (4)$$

where ${}_b\boldsymbol{\omega}_b$ is computed from (2) and ${}_b\dot{\mathbf{x}}_{f_l}, {}_b\mathbf{x}_{f_l}$ are velocity and position of the foot f_l in the base frame, respectively.

To solve the problem of estimating ${}_b\dot{\mathbf{x}}_b$ from each contribution ${}_b\dot{\mathbf{x}}_{b_l}$, we need to know which feet are in stable contact with the ground and to then fuse the individual leg contributions into a single EKF measurement update, with associated covariance.

IV. Contact Estimation

We define the contact status for a foot belonging to leg $l \in \{\text{LF, RF, LH, RH}\}$ as $S_l \in \{0, 1\}$, where 1 indicates a reliable stance (*i.e.,* with no motion relative to the ground) and 0 indicates swing or slipping contact. Let $\mathbf{f}_l$ be the GRF for leg l. This is either measured with some degree of uncertainty or, in our case, computed from the joint position $\mathbf{q}_l$, velocity $\dot{\mathbf{q}}_l$ and effort $\boldsymbol{\tau}_l$, as follows:

$$\mathbf{f}_l = -\left(J_l^{\mathrm{T}}(\mathbf{q}_l)\right)^{-1}\left(\boldsymbol{\tau}_l - \mathbf{h}_l(\mathbf{q}_l, \dot{\mathbf{q}}_l, {}_b\mathbf{g})\right) \quad (5)$$

where $J_l^{\mathrm{T}}(\mathbf{q}_l)$ is the Jacobian transpose from joint to Cartesian space and $\mathbf{h}_l(\mathbf{q}_l, \dot{\mathbf{q}}_l, {}_b\mathbf{g})$ is the vector of Centrifugal/Coriolis/gravity torques for leg l, computed using Recursive Newton-Euler algorithms, as described in [19]. Given the small mass of HyQ's legs compared to the torso, we assume the effect of inertial torques as negligible, compared to the numerical error of computing $\ddot{\mathbf{q}}$.

Given $\mathbf{f}_l = (f_{l,x}, f_{l,y}, f_{l,z})$ and following the definition from [20], the quantity:

$$\mu_f = \frac{\sqrt{f_{l,x}^2 + f_{l,y}^2}}{f_{l,z}}, \quad \forall f_{l,z} > 0 \quad (6)$$

defines a metric to evaluate the robustness of a foothold, in terms of contact stability. This metric is equal to the actual static friction coefficient μ_s when the lateral components of the GRF (denoted with $f_{l,x}, f_{l,y}$) have a value beyond which the foot would start slipping. Although μ_s is unknown, any value of $\mu_f < \mu_s$ would yield a stable contact, and in particular, the smaller μ_f is, the more likely the foot is firmly on the ground. Hence, the quality of contact for a foot related to leg l at time k is non-linearly proportional to $\mathbf{f}_l^k$. For simplicity and numerical stability, instead of accounting for all the terms of μ_s, we ignore the lateral components of $\mathbf{f}_l^k$, and assume that, above a certain threshold of $f_{l,z}^k$, the frictional force will be sufficient to produce a stable, reliable contact.

To learn this threshold, we model the probability of a reliable ground contact P_k using a discriminative logit model:

$$\mathrm{P}_k(S_l = 1 | \mathbf{f}_l^k) = \frac{1}{1 + \exp(-\beta f_{z,l}^k - \beta_0)} \quad (7)$$

where $f_{z,l}^k$ is the normal component of the GRF at time k for leg l, while β and β_0 can be regarded as the weights of a logistic regression classifier. The weights are computed by maximum likelihood estimation on a training set of data collected from characteristic motions, as described next.

A. Fitting With Simulated Data

First, we tested our approach on data generated from simulation, with contact ground truth, for two distinctive locomotion styles: a quasi-static crawl and a dynamic trot.

The crawl gait was obtained from the controller described in [21]. The trot gait was generated using the reactive controller framework presented in [22]. In our experiments the movement was generated using a step frequency of 1.7 Hz, a duty factor of 0.5 and a leg stiffness of 8.55×10^3 Nm^{-1}.

Figs. 2 and 3 show — for crawl and trot datalogs, respectively — the learned logistic function (top plot), the GRF signal (middle plot), and the fitting of the model against the ground truth for the test set (bottom plot). As expected, the threshold for contact activation in the trot gait is higher (by approx. 20 N). This is due to the fact that for this locomotion gait two legs are off the ground at a time, compared to just one in the crawl.

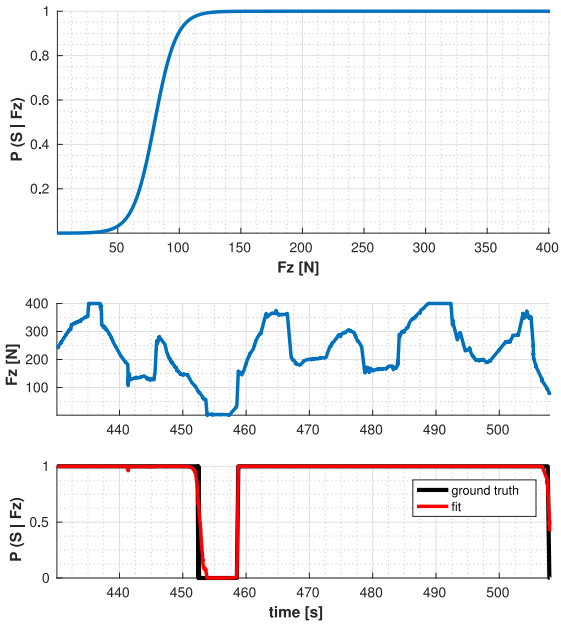

Fig. 2. **Crawl gait simulation.** *Top plot:* learned logistic model function. *Middle plot:* normal component of the GRF for one leg. *Bottom plot:* learned stance probability and ground truth.

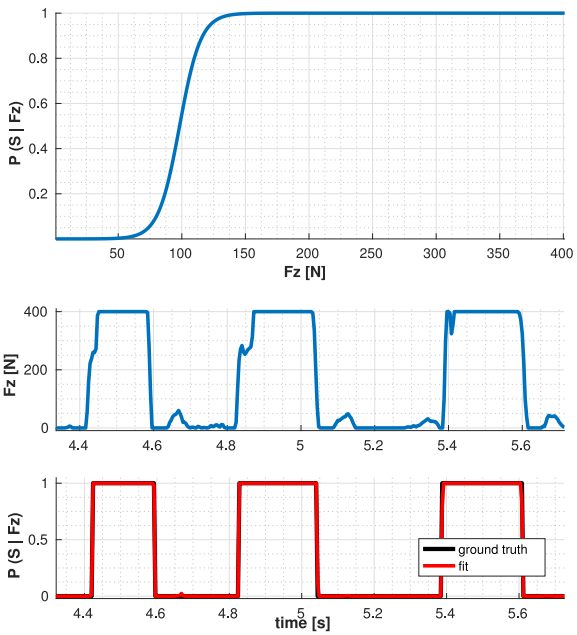

Fig. 3. **Trot gait simulation.** *Top plot:* learned logistic model function. *Middle plot:* normal component of the GRF for one leg. *Bottom plot:* learned stance probability and ground truth.

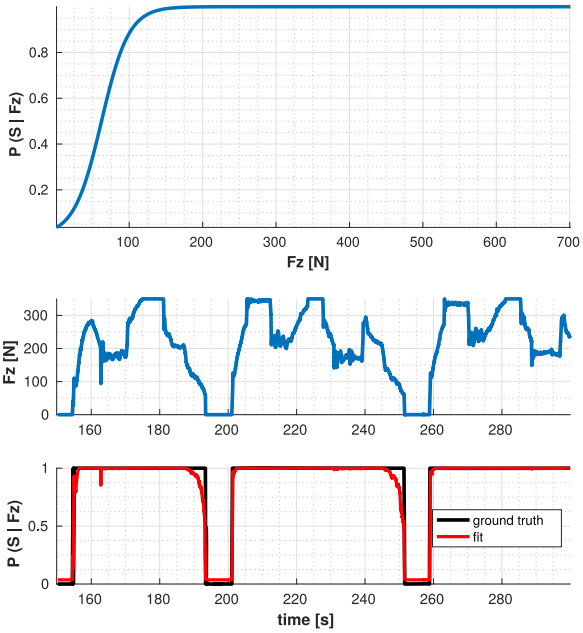

Fig. 4. **Crawl gait experiment.** *Top plot:* learned logistic model function. *Middle plot:* normal component of the GRF for one leg. *Bottom plot:* learned stance probability and ground truth.

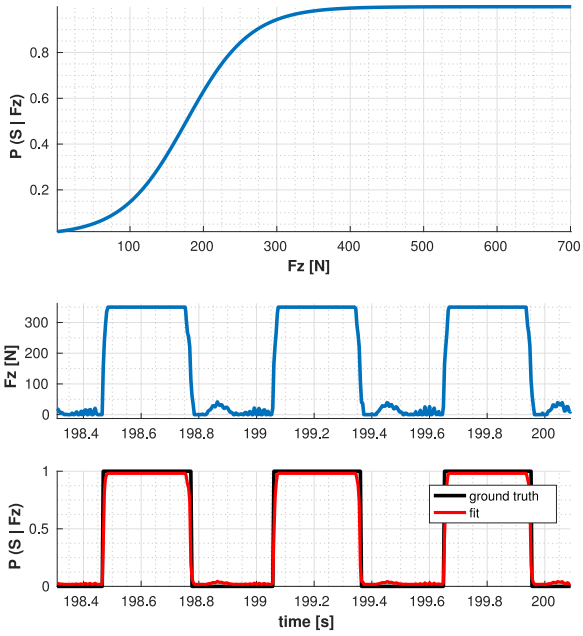

Fig. 5. **Trot gait experiment.** *Top plot:* learned logistic model function. *Middle plot:* normal component of the GRF for one leg. *Bottom plot:* learned stance probability and ground truth.

B. Fitting With Real Data

To test the classifier in a real scenario, we performed training on half of a trot log and half of a crawl log from our dataset (see Section VI-B) and we used the rest of the dataset as a test set for the learned model.

As no suitable commercial solution for contact sensing was available on our hardware, the ground truth for the training was defined as the time sequence of stance leg combinations that minimizes the error between estimated and true base velocities. Additional post-processing was applied to maintain the continuity of the swing and stance intervals. This approach has the advantage that the classifier tends to learn the force threshold beyond which the associated velocity measurement produced by the foot in question becomes reliable.

Figs. 4 and 5 display, for crawl and trot respectively, the obtained logistic function (top plot), the GRF signal (middle

TABLE I
DRIFT PER DISTANCE TRAVELED IN THE x-AXIS OF DIFFERENT CONTACT ESTIMATORS: FIXED THRESHOLD, SCHMITT TRIGGER (HYSTERESIS) AND OUR METHOD (LOGISTIC REGRESSION)

	Fixed threshold [cm m^{-1}]	Hysteresis [cm m^{-1}]	Logistic regr. [cm m^{-1}]
Crawl	1.34	1.34	1.34
Trot	1.79	0.75	0.43

plot), and the fitting of the model against the ground truth for the test set (bottom plot). As in the simulation, the threshold for contact activation in the trot gait is higher.

We compare the state estimation performance using our contact estimation approach against two other thresholding methods on $f_{z,l}$: a single threshold method and a Schmitt trigger. Table I provides an example of how our approach improves the state estimation performance as a function of drift per distance traveled in the x-axis, due to the better selection of the stance legs used for the velocity computation. For these experiments, we decoupled the effect of gyro bias and linear position estimate by using the orientation estimate from a Vicon motion capture system. In particular the proposed logistic regression significantly increases the performance of the LO during the trot gait. For the crawling gait the performance is on a par with the other two methods, as impact events occur less frequently and with reduced intensity.

V. VELOCITY ESTIMATION

Given an estimate of which feet are likely to be in reliable contact, we compute a velocity estimate of the base ${}_b\dot{\mathbf{x}}_b$ and its associated covariance matrix $\Sigma_v = \mathrm{diag}(\sigma_x^2, \sigma_y^2, \sigma_z^2)$ using kinematic sensing. This is then used as a measurement in the EKF update step. To compute the measurement we use the contact estimation method introduced in Section IV, while to compute the covariance we leverage the knowledge about the consistency between the velocity contributions of the stance legs and the detection of impacts.

A. Velocity Computation

To produce a base velocity update for the filter we combine the individual base velocity estimates produced by each leg. We use the probability of a given foot related to leg l being in contact at time k as a weighting criteria as follows:

$$ {}_b\dot{\mathbf{x}}_b(k) = \frac{\sum_{l\in C} \mathrm{P}_k(S_l = 1|\mathbf{f}_l^k)\, {}_b\dot{\mathbf{x}}_{b_l}(k)}{\sum_{l\in C} \mathrm{P}_k(S_l = 1|\mathbf{f}_l^k)} \tag{8} $$

where C is the set of feet that exceed the 0.5 threshold of the logistic regressor. In this way, the feet velocity contribution is weighted proportionally to the probability of contact.

B. Covariance Estimation

Correctly estimating the covariance of these velocity contributions is particularly important. The robot executes different types of dynamic gaits and creates entirely unrealistic velocity updates when a foot strikes the ground.

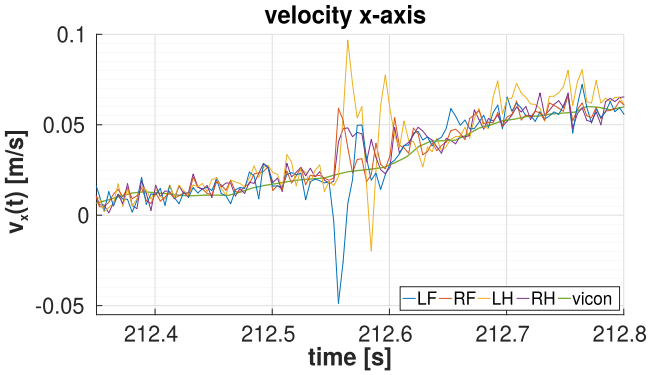

Fig. 6. Effect of impulsive force on estimated velocities during a crawl gait. The Left Hind (LH) leg strikes the ground at time 212.55 s producing unrealistic velocity estimates for that leg — as well as for the other legs, due to propagation of the impact on the rest of the structure.

To compute the covariance matrix Σ_v associated with each velocity update, we considered two factors: consistency between each contribution ${}_b\dot{\mathbf{x}}_{b_l}$ and impact forces. For each coordinate $r \in \{x, y, z\}$ we compute the corresponding variance at a given instant as:

$$ \sigma_r^2(k) = \sigma_0^2 + (\alpha_1 \mathrm{std}\left[{}_b\dot{\mathbf{x}}_{b_{l\in C}}(k)\right]_c + (1-\alpha_1)\alpha_2 |\Delta\bar{f}_z^k|)^2 \tag{9} $$

where:

$$ |\Delta\bar{f}_z^k| = \frac{1}{\dim(C)} \sum_{l\in C} |f_{z,l}^k - f_{z,l}^{k-1}| \tag{10} $$

is the average of the absolute difference between the current and previous normal component of the GRF. We use this value as an indicator of an impact event. σ_0 is the baseline standard deviation for velocity, $\mathrm{std}\left[{}_b\dot{\mathbf{x}}_{b_{l\in C}}\right]$ is the r-th component of the standard deviation of the velocity contributions among stance legs, α_1 is a factor that balances the effects of leg consistency and impacts (we use 0.5) and α_2 is a normalization factor, computed as the ratio between typical velocity error and $|\Delta\bar{f}_z|$ at the same instant.

The middle term of (9) incorporates the fact that legs deemed to be in contact should provide consistent estimates for the same base velocity. The last term takes into consideration the effect of impact forces, which propagate throughout the system and affect also legs that are already in contact (see Fig. 6).

In Fig. 7 we show an example of the adaptive covariance described in this section, on data from a trot log. We compare the raw (*i.e.,* not yet processed by the EKF) base velocity computed from (8) and the ground truth, on the x-axis. The velocity is colored proportionally to the standard deviation $\sigma_x(k)$ extracted from (9). Note the change of color in the proximity of feet contact transitions and impacts, where the standard deviation is increased from 0.02 ms^{-1} up to 0.13 ms^{-1}. During these intervals, the confidence in the velocity updates processed by the EKF is reduced.

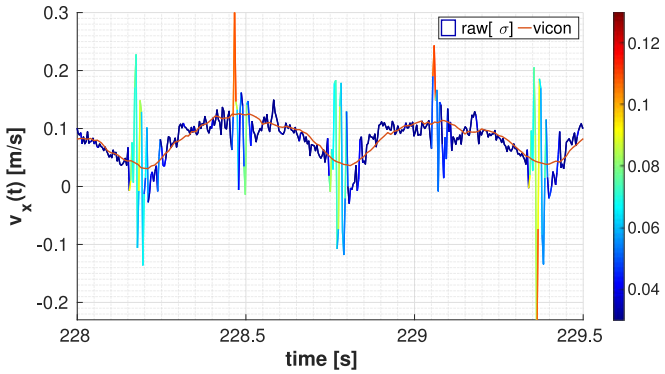

Fig. 7. Raw velocity on x-axis compared to ground truth during a trot motion. The standard deviation associated to the velocity samples is shown with a color scale, ranging from dark blue (0.03 ms^{-1} to dark red 0.13 ms^{-1}).

TABLE II
HYQ SENSOR SPECIFICATIONS

Sensor Type	Model	Accuracy	Rate
IMU	Microstrain GX3-25	0.5° to 2.0°	500 Hz
Rel. Encoders	Avago AEDA3300 BE1	0.0045°	250 Hz
Abs. Encoders	ASM AS5045	0.0879°	250 Hz
Force	Burster 8417	± 25N	250 Hz

TABLE III
SUMMARY OF THE DATASET

Name	Gait	Duration	Distance
trot_1	trot	606 s	38.55 m
trot_2	trot	608 s	40.85 m
trot_3	trot	609 s	48.96 m
walk_1	crawl	395 s	8.05 m
walk_2	crawl	345 s	6.94 m
walk_3	crawl	600 s	10.31 m
walk_4	crawl	600 s	10.89 m

VI. EXPERIMENTS

A. Experimental Platform

The experimental results were obtained on the torque controlled Hydraulic Quadruped robot (HyQ) [4] which is capable of multiple locomotion gaits. The system is 1m long, weighs approximately 85 kg and contains 12 actuated revolute joints with a rotational range of 120° each, with a peak torque of 145 Nm at a hydraulic pressure of 16 MPa. A brief summary of the sensors on the robot, including accuracy and sampling frequency, is provided in Table II. All the sensor inputs except the ones from the IMU are generated at 1 kHz within a real-time environment, sampled at 250 Hz and transmitted as LCM messages to the filter. The IMU is directly accessed in user-space via USB at 500 Hz and synchronized passively [23].

B. Dataset

The dataset we recorded for the experimental tests is summarized in Table III. It consists of seven runs, three of a trotting gait and four of a crawling gait, for a total duration of 62 min. The total distance traveled was computed by path integral of the robot trajectory from Vicon position measurements at 100 Hz. The velocity signals are computed by numerical differentiation and de-noised through a delay-compensated second order Savitzky-Golay filter [24], which was preferred over a moving average because of its smaller signal distortion.

Due to the limited size of our motion capture space, these gaits were performed by repeating forward-backward motions within a 2.5 m^2 × 1.2 m^2 area. Figs. 8(a) and (b) depict a typical trajectory (projected onto the xy-plane) of a crawl and a trot run, respectively.

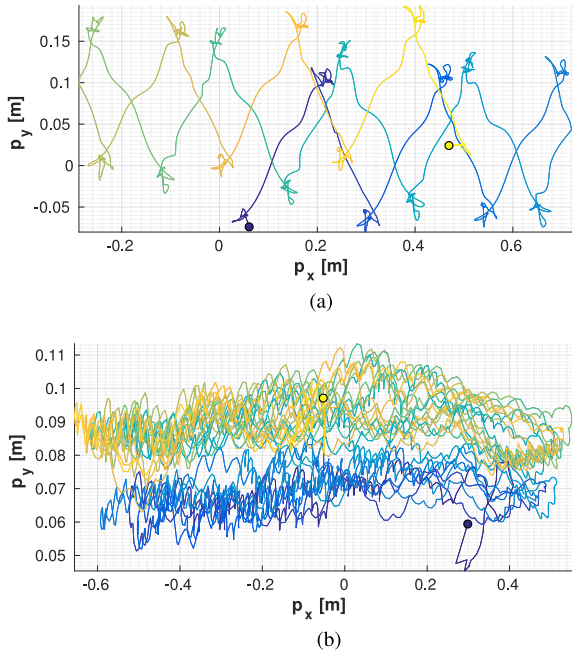

Fig. 8. Typical crawl and trot base trajectories, projected on the xy-plane. Color changes from dark blue to light yellow indicate the evolution of time. Starting and ending positions are indicated by a blue and a yellow dot, respectively.

C. Performance Evaluation

Fig. 9 compares, for a forward trot, the velocity estimates before filtering (top plot), after filtering (middle plot) and the ground truth (bottom plot). Despite several spikes due to impacts, the filtered output is smooth, thanks to the adaptive covariance algorithm presented in Section V, which automatically reduces the confidence on the kinematics filter updates during stance transitions.

In Figs. 10 and 11 we show the average performance on the dataset presented in Section VI-B, of the trot and crawl logs, for each coordinate. In Fig. 10 we evaluate the Drift per Distance Traveled (DDT), *i.e.,* the mean position drift divided by the total distance covered by the robot. Fig. 11 shows the Root Mean Square error (RMS) of the velocity estimates. We compared the proposed algorithm (yellow bars) with a simple method based on a fixed threshold of 50 N on the normal component of the GRF for contact detection, and static covariance for the velocity updates (dark blue bars).

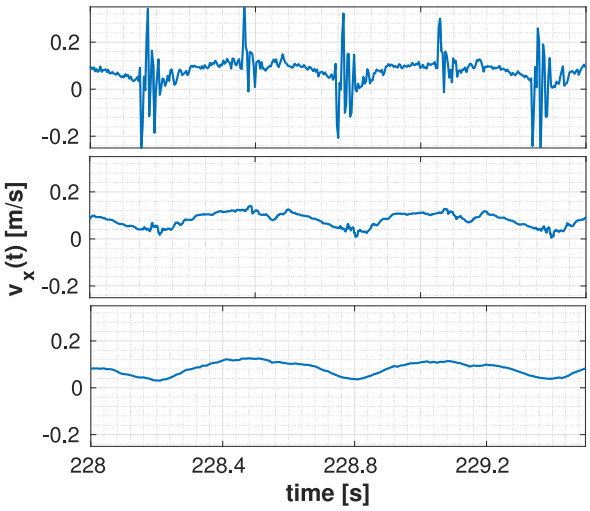

Fig. 9. Example of velocity estimation for a trot log on x-axis. *Top plot:* raw velocity. *Middle plot:* output of the EKF. *Bottom plot:* ground truth.

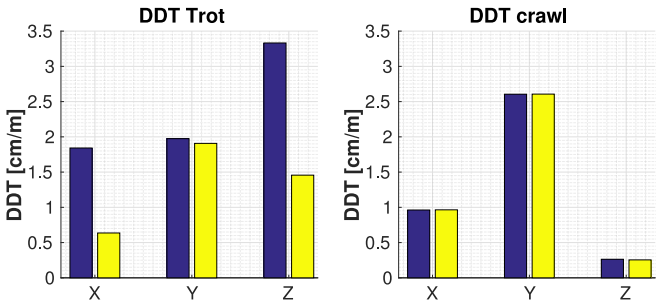

Fig. 10. Drift per Distance Traveled (DDT) for trot and crawl logs. Left blue bars show the baseline method, right yellow bars show our approach.

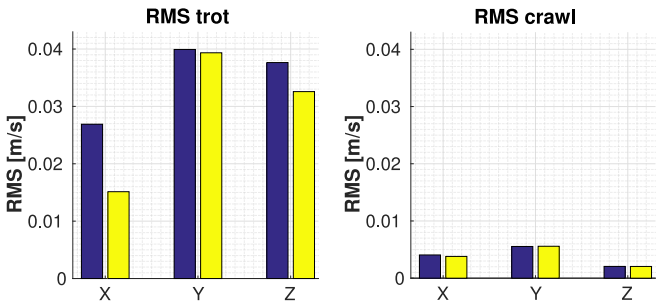

Fig. 11. Velocity Root Mean Square (RMS) error for trot and crawl logs. Left blue bars show the baseline method, right yellow bars show our approach.

Although the two gaits we used for our tests differ considerably, for both we noticed a performance degradation on the y-axis, an issue we attribute to structural flexibility of the leg (see Section VII for more details).

1) Trot logs: For the trotting logs (left-hand sides of Figs. 10 and 11), we demonstrate that properly handling impacts improves significantly the performance both in position and velocity. We have achieved this in the x and the z axes, where the error in position is more than halved with respect to the simple method (dark blue bars). In the y axis the same performance improvement was not achieved due to limb flexibility, as explained in Section VII.

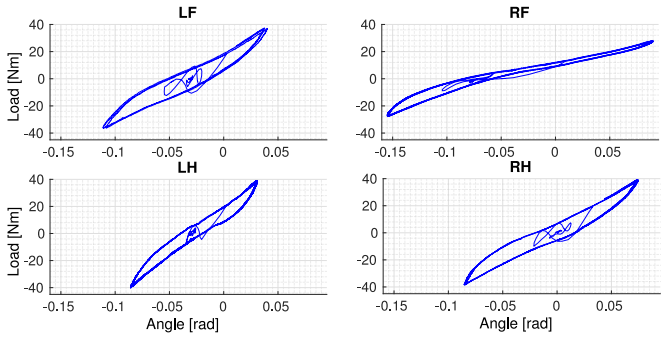

Fig. 12. Joint Load versus Position plots for the four legs under loading/unloading produced at each foot on the y-axis. Hysteresis indicates nonlinear elasticity and energy dissipation between loading and unloading phases.

2) Crawling: The plots on the right-hand side of Figs. 10 and 11 show the two main performance indicators for the crawling logs. As expected, given the sporadic occurrence of impacts, the improvement provided by our proposed approach is limited. We can notice how the error on the z component is lower than for the trot because of the continuous support typical for this gait.

VII. Discussion

A. Leg Flexibility Under Load

Large robots like HyQ can exhibit undesired leg compliance and flexibility when their feet strike the ground, even at slow speeds. Typical forces at the feet are in the range of 200 N to 600 N while crawling or trotting, and beyond 1200 N while bounding. These forces are partially absorbed by the leg structure.

A dedicated experiment allowed us to identify that the major cause of performance degradation along the y-axis (shown in Figs. 10 and 11) is the intrinsic flexibility of the legs on the coronal plane. With the robot base fixed in place and the feet firmly in contact with the ground, we controlled the legs to produce lateral forces at the feet along the y-axis using a triangular wave with period of 20 s and intensity of 70 N. Fig. 12 shows the relationship between position and applied torque at Hip Abduction Adduction (HAA) joints (*i.e.,* joints rotating around an axis passing through the hip and aligned with the x-axis). It highlights the nonlinearity of the leg structure and the hysteresis between loading and unloading phases. Given the configuration of the experiment, the joint motion should have been very small, but a range up to 0.24 rad is recorded (see widths of the graphs in Fig. 12). This indicates significant structural flexibility.

Methods to model this nonlinearity so as to achieve the same state estimation performance for the y-axis as obtained for the x and z axes is ongoing research, as well as testing the approach on the second version of HyQ, called HyQ2Max [25], which is expected to show a better structural behavior.

B. Limitations

Besides the mechanical structure of the robot, limitations lie in: a) the training of the contact classifier and b) terrain

properties. A specific training procedure was required for each gait, and would be needed for every new gait or loading condition for the legs. This could be avoided by performing unsupervised learning and active exploration of terrain frictional properties, but at the current stage only tests in controlled single leg setups have been reported in literature [20]. Alternatively, simulation could provide a set of parameters for a sufficient number of cases to generalize the applicability of the approach.

Concerning the terrain properties, in order to correctly estimate contacts, GRFs need to be projected on the local plane where the foot is experiencing the contact. Although this can be done in first approximation by fitting a plane through the current or recent stance feet positions, more sophisticated methods (using exteroception) are required when the terrain inclination changes significantly within the support region. Other terrain properties, like elasticity or plasticity, are not explicitly accounted for, but a contact model for specific terrain classes can be learned through the proposed approach.

VIII. Conclusion and Future Work

In this paper we presented a novel probabilistic approach to contact estimation for state estimation of dynamic legged robots without contact sensing. The approach uses a logistic classifier to learn the GRF threshold which has the highest probability so as to minimize the base velocity error. Additionally, we presented an algorithm which merges the velocity contributions of the individual legs, using their probabilistic contact information, to create the main measurement update for our combined filter [11].

We have demonstrated that the combination of these two algorithms can double the performance in position and velocity, compared to standard methods, and can compensate for a lack of dedicated contact sensors at the feet.

The presented methodology was developed and extensively tested with more than one hour of testing data from a quadrupedal robotic platform without contact sensors, in both quasi-static and dynamic locomotion regimes.

Our future work includes the integration of exteroceptive modules to further improve the performance during field trials. It would also be interesting to extend our approach to robots equipped with contact sensors so as to provide redundancy in case of sensor noise or damage.

Acknowledgment

The authors would like to thank all members of the Dynamic Legged System Laboratory for their valuable help.

References

[1] G. P. Roston and E. Krotkov, "Dead reckoning navigation for walking robots," Robot. Inst., Pittsburgh, PA, USA, Tech. Rep. CMU-RI-TR-91-27, Nov. 1991.

[2] P. Sardain and G. Bessonnet, "Forces acting on a biped robot. Center of pressure-zero moment point," *IEEE Trans. Syst., Man Cybern. A, Syst. Humans*, vol. 34, no. 5, pp. 630–637, Sep. 2004.

[3] A. Bowling, "Impact forces and mobility in legged robot locomotion," in *Proc. IEEE/ASME Int. Conf. Adv. Intell. Mechatronics*, Sep. 2007, pp. 1–8.

[4] C. Semini, N. G. Tsagarakis, E. Guglielmino, M. Focchi, F. Cannella, and D. G. Caldwell, "Design of HyQ—A hydraulically and electrically actuated quadruped robot," *Proc. Inst. Mech. Eng., Part I: J. Syst. Control Eng.*, vol. 225, no. 6, pp. 831–849, 2011.

[5] P.-C. Lin, H. Komsuoglu, and D. E. Koditschek, "Sensor data fusion for body state estimation in a hexapod robot with dynamical gaits," *IEEE Trans. Robot.*, vol. 22, no. 5, pp. 932–943, Oct. 2006.

[6] M. Görner and A. Stelzer, "A leg proprioception based 6 DOF odometry for statically stable walking robots," *Auton. Robots*, vol. 34, no. 4, pp. 311–326, 2013.

[7] A. Chilian, H. Hirschmüller, and M. Görner, "Multisensor data fusion for robust pose estimation of a six-legged walking robot," in *Proc. IEEE/RSJ Int. Conf. Intell. Robot. Syst.*, 2011, pp. 2497–2504.

[8] M. Bloesch *et al.*, "State estimation for legged robots—Consistent fusion of leg kinematics and IMU," in *Proc. Robot. Sci. Syst.*, Sydney, Australia, Jul. 2012, pp. 17–24.

[9] M. Hutter, C. Gehring, M. Bloesch, M. A. Hoepflinger, C. D. Remy, and R. Siegwart, "StarlETH: A compliant quadrupedal robot for fast, efficient, and versatile locomotion," in *Proc. 15th Int. Conf. Climbing Walking Robots*, 2012, pp. 483–490.

[10] M. Bloesch, C. Gehring, P. Fankhauser, M. Hutter, M. Hoepflinger, and R. Siegwart, "State estimation for legged robots on unstable and slippery terrain," in *Proc. IEEE/RSJ Int. Conf. Intell. Robot. Syst.*, Nov. 2013, pp. 6058–6064.

[11] M. Fallon, M. Antone, N. Roy, and S. Teller, "Drift-free humanoid state estimation fusing kinematic, inertial and LIDAR sensing," in *Proc. 14th IEEE-RAS Int. Conf. Humanoid Robots*, Nov. 2014, pp. 112–119.

[12] E. Parr, "Digital control systems," in *Electrical Engineer's Reference Book*, 16th ed., M. Laughton and D. Warne, Eds. New York, NY, USA: Newnes, 2003, pp. 1–36.

[13] M. Frigerio, J. Buchli, D. G. Caldwell, and C. Semini, "RobCoGen: A code generator for efficient kinematics and dynamics of articulated robots, based on domain specific languages," *J. Softw. Eng. Robot.*, vol. 7, no. 1, pp. 36–54, 2016.

[14] J. Ma, M. Bajracharya, S. Susca, L. Matthies, and M. Malchano, "Real-time pose estimation of a dynamic quadruped in GPS-denied environments for 24-hour operation," *Int. J. Robot. Res.*, vol. 35, no. 5, pp. 631–653, 2015.

[15] A. D. Luca, A. Albu-Schaffer, S. Haddadin, and G. Hirzinger, "Collision detection and safe reaction with the DLR-III lightweight manipulator arm," in *Proc. IEEE/RSJ Int. Conf. Intell. Robot. Syst.*, Oct. 2006, pp. 1623–1630.

[16] S. Haddadin, A. Albu-Schaffer, A. D. Luca, and G. Hirzinger, "Collision detection and reaction: A contribution to safe physical Human-Robot Interaction," in *Proc. IEEE/RSJ Int. Conf. Intell. Robot. Syst.*, Sep. 2008, pp. 3356–3363.

[17] J. Hwangbo, C. D. Bellicoso, P. Fankhauser, and M. Hutter, "Probabilistic foot contact estimation by fusing information from dynamics and differential/forward kinematics," in *Proc. IEEE/RSJ Int. Conf. Intell. Robot. Syst.*, Oct. 2016, pp. 3872–3878.

[18] T. D. Greenwood, *Advanced Dynamics*, Cambridge University Press, Nov. 2003, Chap. 1.

[19] R. Featherstone, *Robot Dynamics Algorithms*. Norwell, MA, USA: Kluwer, 1987.

[20] M. A. Hoepflinger, M. Hutter, C. Gehring, M. Bloesch, and R. Siegwart, "Unsupervised identification and prediction of foothold robustness," in *Proc. IEEE Int. Conf. Robot. Autom.*, May 2013, pp. 3293–3298.

[21] M. Focchi, A. del Prete, I. Havoutis, R. Featherstone, D. G. Caldwell, and C. Semini, "High-slope terrain locomotion for torque-controlled quadruped robots," *Auton. Robots*, vol. 41, no. 1, pp. 259–272, 2017.

[22] V. Barasuol, J. Buchli, C. Semini, M. Frigerio, E. R. D. Pieri, and D. G. Caldwell, "A reactive controller framework for quadrupedal locomotion on challenging terrain," in *Proc. IEEE Int. Conf. Robot. Autom.*, May 2013, pp. 2554–2561.

[23] E. Olson, "A passive solution to the sensor synchronization problem," in *Proc. IEEE/RSJ Int. Conf. Intell. Robot. Syst.*, Oct. 2010, pp. 1059–1064.

[24] A. Savitzky and M. J. E. Golay, "Smoothing and differentiation of data by simplified least squares procedures," *Analytical Chem.*, vol. 36, no. 8, pp. 1627–1639, 1964.

[25] C. Semini *et al.*, "Design of the hydraulically-actuated, torque-controlled quadruped robot HyQ2Max," *IEEE/ASME Trans. Mechatronics*, vol. PP, no. 99, p.1, 2016.